Atmos. Chem. Phys., 22, 4951–4967, 2022
https://doi.org/10.5194/acp-22-4951-2022

Atmospheric Chemistry and Physics
Open Access
EGU

Formation, radiative forcing, and climatic effects of severe regional haze

Yun Lin[1,2], Yuan Wang[3], Bowen Pan[1,4], Jiaxi Hu[1,5], Song Guo[6], Misti Levy Zamora[1,7], Pengfei Tian[1,8], Qiong Su[9], Yuemeng Ji[1,10], Jiayun Zhao[11], Mario Gomez-Hernandez[11], Min Hu[6], and Renyi Zhang[1,11]

[1]Department of Atmospheric Sciences, Texas A&M University, College Station, TX 77843, USA
[2]Joint Institute for Regional Earth System Science and Engineering (JIFRESSE), University of California at Los Angeles, Los Angeles, CA 90064, USA
[3]Division of Geological and Planetary Sciences, California Institute of Technology, Pasadena, CA 91125, USA
[4]Department of Atmospheric Science, Colorado State University, Fort Collins, CO 80521, USA
[5]Cooperative Institute for Mesoscale Meteorological Studies, NOAA/OAR National Severe Storms Laboratory, Norman, OK, USA
[6]State Key Joint Laboratory of Environmental Simulation and Pollution Control, College of Environmental Sciences and Engineering, Peking University, Beijing, 10087, PR China
[7]Department of Public Health Sciences, School of Medicine, University of Connecticut, Farmington, CT 06030-6325, USA
[8]Key Laboratory for Semi-Arid Climate Change of the Ministry of Education, College of Atmospheric Sciences, Lanzhou University, Lanzhou 730000, PR China
[9]Water Management & Hydrological Science, Texas A&M University, College Station, TX 77843, USA
[10]Guangzhou Key Laboratory of Environmental Catalysis and Pollution Control, School of Environmental Science and Engineering, Institute of Environmental Health and Pollution Control, Guangdong University of Technology, Guangzhou 510006, China
[11]Department of Chemistry, Texas A&M University, College Station, TX 77843, USA

Correspondence: Yun Lin (yunlin@ucla.edu), Yuan Wang (Yuan.Wang@caltech.edu), and Renyi Zhang (renyi-zhang@tamu.edu)

Received: 22 September 2021 – Discussion started: 29 October 2021
Revised: 16 February 2022 – Accepted: 17 March 2022 – Published: 14 April 2022

Abstract. Severe regional haze events, which are characterized by exceedingly high levels of fine particulate matter (PM), occur frequently in many developing countries (such as China and India), with profound implications for human health, weather, and climate. The occurrence of the haze extremes involves a complex interplay between primary emissions, secondary formation, and conducive meteorological conditions, and the relative contributions of the various processes remain unclear. Here we investigated severe regional haze episodes in 2013 over the Northern China Plain (NCP), by evaluating the PM production and the interactions between elevated PM and the planetary boundary layer (PBL). Analysis of the ground-based measurements and satellite observations of PM properties shows nearly synchronized temporal PM variations among the three megacities (Beijing, Baoding, and Shijiazhuang) in this region and a coincidence of the aerosol optical depth (AOD) hotspots with the three megacities during the polluted period. During the clean-to-hazy transition, the measured oxygenated organic aerosol concentration ([OOA]) well correlates with the odd-oxygen concentration ($[O_x] = [O_3] + [NO_2]$), and the mean $[OOA] / [O_x]$ ratio in Beijing is much larger than those in other megacities (such as Mexico City and Houston), indicating highly efficient photochemical activity. Simulations using the Weather Research and Forecasting (WRF) model coupled with an explicit aerosol radiative module reveal that strong aerosol–PBL interaction during the polluted period results in a suppressed and stabilized PBL and elevated humidity, triggering a positive feedback to amplify the haze severity at the ground level. Model sensitivity study illustrates the importance of black carbon (BC) in the haze–PBL interaction and the aerosol regional climatic effect, contributing to

more than 30 % of the PBL collapse and about half of the positive radiative forcing on the top of the atmosphere. Overall, severe regional haze exhibits strong negative radiative forcing (cooling) of -63 to $-88\,\mathrm{W\,m^{-2}}$ at the surface and strong positive radiative forcing (warming) of 57 to $82\,\mathrm{W\,m^{-2}}$ in the atmosphere, with a slightly negative net radiative forcing of about $-6\,\mathrm{W\,m^{-2}}$ on the top of the atmosphere. Our work establishes a synthetic view for the dominant regional features during severe haze events, unraveling rapid in situ PM production and inefficient transport, both of which are amplified by atmospheric stagnation. On the other hand, regional transport sufficiently disperses gaseous aerosol precursors (e.g., sulfur dioxide, nitrogen oxides, volatile organic compounds, and ammonia) during the clean period, which subsequently result in rapid in situ PM production via photochemistry during the transition period and via multiphase chemistry during the polluted period. Our findings highlight the co-benefits for reduction in BC emissions, which not only improve local and regional air quality by minimizing air stagnation but also mitigate the global warming by alleviating the positive direct radiative forcing.

1 Introduction

Rapid economic growth and urbanization have caused frequent severe regional haze events associated with heavy pollution of particulate matter (PM) in many developing countries, including China and India (Bouarar et al., 2017; Molina, 2021). The severe haze events induce great degradation in visibility and air quality, with profound societal implications (An et al., 2019). For example, exposure to elevated levels of fine PM leads to adverse health effects, ranging from aggravated allergies to the development of chronic diseases, to premature death (Pope and Dockery, 2006; Wu et al., 2019; Rychlik et al., 2019; Johnson et al., 2021; Zhang et al., 2021). Also, elevated levels of fine aerosols result in pronounced modifications to clouds, precipitation, and lightning, impacting regional/global weather and climate (Zhang et al., 2007; Yuan et al., 2008; Qian et al., 2009; Wang et al., 2011; Y. S. Wang et al., 2014; Wu et al., 2016). Specifically, by absorbing/scattering solar radiation, aerosols impact the atmospheric stability and the energy budget of Earth, via the aerosol–radiation interaction (ARI). By serving as cloud condensation nuclei (CCN) and ice nucleating particles (INPs), aerosols influence the macro- and microphysical properties of clouds, via the aerosol–cloud interaction (ACI). Currently, the radiative forcing associated with ARI and ACI represents the largest uncertainty in the projection of future climate by anthropogenic activities (IPCC, 2013).

PM is either emitted directly into the atmosphere (primary) or produced in air via gas-to-particle conversion (secondary) (Zhang et al., 2015b). Primary and secondary PM also undergo chemical and physical transformations and are subjected to cloud processing and removal from air (Zhang et al., 2015b). Direct emissions of primary gases and PM and highly efficient secondary PM formation represent the primary processes leading to severe haze (Guo et al., 2014; Sun et al., 2014; G. Wang et al., 2016). Haze evolution typically exhibits distinctive secondary aerosol formation, which is linked to several chemical and physical processes, that is, new particle formation and aerosol growth driven by photochemistry during the clean stage and aqueous chemistry during the transition stage as well as the interaction between aerosols and atmospheric stability relevant to solar radiation absorption (Zhang et al., 2009; Xu and Zhang, 2012; Ji et al., 2020; Peng et al., 2021). In addition, conducive weather conditions for pollutant accumulation, such as regional control by high-pressure, suppressed local circulations, and weakened large-scale circulation, correspond to the external causes for severe haze formation (Liu et al., 2013; Y. S. Wang et al., 2014; Cai et al., 2017; Li et al., 2019).

The key constituents of fine PM include secondary inorganic (including sulfate, nitrate, and ammonium) aerosol (SIA) and secondary organic aerosol (SOA), with the corresponding gaseous precursors of sulfur dioxide (SO_2), nitrogen oxides ($NO_x = NO + NO_2$), ammonia (NH_3), and volatile organic compounds (VOCs). The photochemistry represents one of the mechanisms leading to SIA and SOA accumulation during the early stage of haze evolution (Guo et al., 2014; Zhang et al., 2015b, 2020; G. Wang et al., 2016). Field measurements have shown that remarkably nucleation and growth of nanoparticles are primarily driven by photochemical activity, which is characterized by elevated ozone levels and efficient photolysis rate coefficients under clean daytime conditions (Zhang et al., 2015a; Guo et al., 2020). During haze evolution, the photochemical activity is typically reduced, as evident by low levels of ozone and reduced photolysis rates (Peng et al., 2021). On the other hand, there are increasing air stagnation and relative humidity (RH), when explosive secondary aerosol formation occurs (Peng et al., 2021). The latter has been attributed the occurrence of multiphase chemistry, which largely drives the formation of SIA and SOA during the polluted period (Peng et al., 2021). Currently, the relative contributions of primary emissions, secondary production, and regional transport to severe haze formation remain uncertain (Li et al., 2015; Zhang et al., 2015a; Peng et al., 2021). Moreover, the efficiency of photochemical PM production during regional haze events in the Northern China Plain (NCP) and its distinction among var-

ious megacities worldwide remain to be quantified (Molina, 2021).

While the importance of regional haze on climate has been recognized (Ramanathan et al., 2007; Wang et al., 2009; H. Wang et al., 2015), there still lacks quantification for the aerosol radiative forcing and the climatic effects for severe regional haze events. Estimation of the aerosol radiative forcing during severe haze events exhibits a large variation (Li et al., 2007; Xia et al., 2007; Wang et al., 2009; Che et al., 2014). In addition, the interactions between aerosols and planetary boundary layer (PBL) via the aerosol radiative effects likely increase the haze severity (H. Wang et al., 2015; J. Wang et al., 2016; Zhang et al., 2018). Meteorological conditions within the PBL, including the atmospheric stability and RH, are altered by the aerosol–PBL interaction to induce a positive feedback to PM accumulation near the ground level (G. Tang et al., 2016; Tie et al., 2017; Wu et al., 2020). However, the aerosol–PBL interactions and their feedbacks to atmospheric thermodynamics and dynamics under extremely hazy conditions remain to be quantified (Li et al., 2017).

Previous studies have documented the role of black carbon (BC) in the aerosol–PBL interactions and the aerosol regional climate effects (Menon et al., 2002; Bond et al., 2013; Wang et al., 2013; Ding et al., 2016). In addition, the BC aging process markedly enhances BC absorption by modifying the particle physiochemical and optical properties (Zhang et al., 2008; Khalizov et al., 2013; He et al., 2015; Guo et al., 2016; Peng et al., 2016, 2017). For example, an experimental/field study showed that the mass absorption cross section (MAC) of BC is enhanced by 2.4 times in a short time because of BC aging under polluted urban conditions (Peng et al., 2016), reconciling previous variable results on the coating-enhanced absorption for BC (Gustafsson and Ramanathan, 2016). Apparently, the enhancement of the BC absorption causes additional aerosol radiative forcing (Peng et al., 2016) and suppression on PBL development (Wang et al., 2018). Currently, limited modeling studies have assessed the radiative effect of BC aging associated with severe regional haze (Wang et al., 2013; He et al., 2015; Gustafsson and Ramanathan, 2016).

To better understand the formation and evolution of severe regional haze as well as their regional and climate effects, we investigated severe haze episodes occurring in 2013 over the Northern China Plain (NCP). The NCP region, which encompasses the megacities of Beijing and Tianjin, and some portion of the provinces of Hebei, Shandong, and Henan, represents the most polluted area in China (An et al., 2019). Satellite observations and field measurements of PM properties were evaluated, and numerical simulations were performed to elucidate the interactions between severe haze and PBL using Weather Research and Forecast (WRF) model coupled with an explicit aerosol radiative module (Fan et al., 2008; Y. Wang et al., 2014a). By conducting model sensitivity simulations, we elucidated the impacts of BC aging on the haze–PBL interactions and its contribution to the net aerosol radiative forcing during severe haze periods.

2 Methodology

The NCP represents a key economic zone in China, as reflected by its gross domestic product (GDP), energy consumption, and vehicular fleets (An et al., 2019). The region has undergone fast industrialization and urbanization over the past 4 decades. For example, the NCP is one of the most densely populated regions in the world and contributes to over 1/10 of the GDP in China. The consumption of coal and crude oil in the NCP was 363 and 72×10^6 t, respectively, to 1348×10^6 t in 1998 and increased to 140×10^6 t of standard coal equivalent in 2010, respectively. In particular, anthropogenic activities result in industrial, traffic, residential, and agricultural emissions, representing the major sources for PM precursors, including SO_2, NO_x, VOCs, and NH_3 (An et al., 2019; Peng et al., 2021). Surrounded by the Taihang Mountains to the west and Yan Mountains to the north, respectively, the NCP region is prone to develop air stagnation under conducive meteorological conditions, inhibiting vertical and horizontal dispersion of air pollutants (An et al., 2019; Peng et al., 2021).

2.1 The data sources

The satellite-retrieved aerosol optical depth (AOD) was derived by combining the Moderate Resolution Imaging Spectroradiometer (MODIS) measurements of Aqua and Terra using the equal-weighted mean method to increase the spatial coverage (Levy et al., 2009). The MODIS data are accessible at https://giovanni.gsfc.nasa.gov/giovanni/ (last access: 12 January 2021; Platnick, 2017). The Terra visible images were obtained at https://worldview.earthdata.nasa.gov/ (last access: 12 January 2021). The hourly PBL height used was based on the Modern-Era Retrospective analysis for Research and Applications, Version 2 (MERRA2) reanalysis data. The severe haze days were selected with daily $PM_{2.5}$ (particular matter with aerodynamic diameter less than 2.5 µm) concentration greater than $200\,\mu g\,m^{-3}$, and the typical clean days were limited to the days with daily $PM_{2.5}$ concentration smaller than $30\,\mu g\,m^{-3}$. The PBL height and the $PM_{2.5}$ surface concentration at 14:00 Beijing time (BJT) each day in 2013 were used for the correlation analysis. All raining days were filtered out when analyzing the correlation between the PBL height and the $PM_{2.5}$ concentration. The surface solar radiation (SSR) data were based on the satellite retrievals (W. Tang et al., 2016), which are accessible at http://www.tpedatabase.cn (last access: 12 January 2021).

Ground-based measurements of fine particulate matter or $PM_{2.5}$ employed in our analysis covered the period from 25 September to 14 November 2013. The hourly $PM_{2.5}$ concentrations in Beijing (BJ) were obtained from the Embassy of United States in Beijing (http://www.stateair.net/web/

historical/1/1.html, last access: 12 January 2021). The $PM_{2.5}$ mass concentrations in Baoding (BD) and Shijiazhuang (SJZ) were obtained from https://air.cnemc.cn:18007/ (last access: 12 January 2021). Measurements of PM properties in Beijing were taken from that previously reported by Guo et al. (2014), which provided $PM_{2.5}$ concentration, aerosol chemical composition, and gaseous data for correlation analysis and constrains for modeling studies. For example, the mass concentrations of various inorganic and organic aerosol species, including oxygenated organic aerosol (OOA), were measured using an aerosol mass spectrometer (AMS) in Beijing (Aiken et al., 2009; Guo et al., 2014). The observation-based analysis and the modeling study focused on two severe haze episodes, i.e., 25 September–30 September (episode 1 or EP1) and 2 October–6 October (episode 2 or EP2) 2013 in the NCP.

2.2 Model experiments

2.2.1 Simulations on the haze–PBL interactions

The aerosol–PBL interactions during the severe haze events and the associated regional climate effects were examined by conducting WRF modeling sensitivity studies. An aerosol radiative module was implemented by Fan et al. (2008) to the Goddard Shortwave Radiation Scheme to online compute the wavelength-dependent aerosol optical properties, including the AOD, the asymmetry factor, and the single scattering albedo (SSA). Aerosol particles with the core-shell configuration in the aerosol radiative module were assumed to consist of BC (core) and ammonia sulfate (shell). The hygroscopic growth of aerosol particles was taken into account, following Mallet et al. (2004). A two-moment bulk microphysical scheme developed by Li et al. (2008) was employed, which has been widely used to investigate the aerosol–cloud interactions under various cloud systems (Y. Wang et al., 2014b, c; Lin et al., 2016). A 100×100 grid domain with a horizontal grid spacing of 2 km and 50 vertical levels with stretched grid spacings was set up to cover the entire urban region of Beijing. The initial and boundary meteorological conditions were generated from six-hourly NCEP FNL (Final) Operational Global Analysis ($1^\circ \times 1^\circ$). No convective parametrization was applied for the simulations.

We performed simulations on the two haze episodes (EP1 and EP2). The 2 days prior to the two haze episodes (25 September and 2 October 2013) are denoted as the clean periods, while the most-polluted days during the two episodes (i.e., 28 September and 5 October) are denoted as the polluted periods. The aerosol number size distributions for initial and boundary conditions of all simulation were based on the measurements during the 2013 field campaign in Beijing (Fig. S1 in the Supplement). The aerosol measurements on 25 September and 2 October 2013 were taken as the input for the clean cases and 28 September and 5 October 2013 for the polluted cases. The aerosol surface number and mass concentration for modeling initialization were set as $3.5 \times 10^4\,\mathrm{cm}^{-3}$ ($3.6 \times 10^4\,\mathrm{cm}^{-3}$) and $10\,\mu\mathrm{g\,m}^{-3}$ ($11\,\mu\mathrm{g\,m}^{-3}$) for the clean case of EP1 (EP2) and $1.7 \times 10^4\,\mathrm{cm}^{-3}$ ($1.8 \times 10^4\,\mathrm{cm}^{-3}$) and $280\,\mu\mathrm{g\,m}^{-3}$ ($310\,\mu\mathrm{g\,m}^{-3}$) for the polluted case of EP1 (EP2), respectively, consistent with the field measurements. Also, based on the measurements, the BC percentage in total aerosol mass was set as 10.0 % and 6.0 % for the clean and polluted cases, respectively. The 2 polluted days for simulations were cloud-free days; therefore the aerosol indirect effects were ruled out.

To assess the role of BC in the aerosol suppression effect on the PBL development and the aerosol radiative forcing during haze evolution, we performed a set of sensitivity simulations under the polluted condition by excluding the BC effects (referred as non-BC case), in which the BC radiative effect was turned off by assigning a zero value to the real and imaginary parts of BC refractive index (i.e., the SSA in non-BC case was equal to unity). To quantify the BC aging effects, additional simulations were carried out for fresh BC (denoted by fresh-BC), in which the BC core was not imbedded in the non-BC shell and the optical parameters for the BC and non-BC components were calculated separately by the Mie theory. In the fresh-BC case, the lensing effect due to the coating during the aging process was excluded, but the restructuring effect induced by aging was considered partially since the BC core was assumed to be spherical and in the compact shape. Alternatively, a case for aged BC (denoted by aged-BC) was treated by considering the full aerosol components (with both BC and non-BC components) and the core-shell configuration. A summary of the simulation cases is listed in Table 1.

One deficiency to predict the absorbed AOD and the directive radiation forcing of BC in atmospheric models is relevant to the underestimation in coating-enhancement of BC absorption (Bond et al., 2013). To assess the potential bias on the radiative effects of aged BC, additional simulations on the polluted conditions were conducted by constraining the enhancement of mass absorption cross section of BC ($E_{\mathrm{MAC\text{-}BC}}$) according to the experimental value, i.e., 2.4, derived from a chamber study in Beijing (Peng et al., 2016). Though the $E_{\mathrm{MAC\text{-}BC}}$ of 2.3 derived from the aged-BC case is slightly lower than that reported by Peng et al. (2016), comparison between the two simulations indicates little difference in the thermodynamic/dynamic conditions and the radiative budget.

2.2.2 Empirical estimation of the moisture effect on haze–PBL interactions

In addition to the numerical model simulations, we employed an empirical equation derived by Nozaki (1973) and modified by Tie et al. (2017) to examine the RH sensitivity in the boundary layer to the PBL height based on observed meteo-

Table 1. List of numerical experiments.

Case	Description
clean	Simulations with aerosol conditions from the days just before the two selected haze episodes start (25 September and 2 October 2013), with daily mean $PM_{2.5} < 30\,\mu g\,m^{-3}$.
aged-BC	Simulations on the most polluted days during the two haze episodes (28 September and 5 October 2013), with daily mean $PM_{2.5} > 200\,\mu g\,m^{-3}$. The core-shell configuration is assumed for BC and non-BC component mixing. The BC core is assumed as a sphere.
non-BC	The polluted cases but without BC radiative effects by turning off calculations of BC absorption and scattering.
fresh-BC	The polluted cases with fresh BC, in which the BC core is assumed as a sphere but not imbedded in the non-BC shell. The optical properties of the BC core are calculated externally using a Mie theory code. The lensing effect due to aging is not considered in this case.

rological conditions:

$$H = \frac{121}{6}(6-P)(T-T_d) + \frac{0.169P(U_Z+0.257)}{12f\ln Z/z_0}, \quad (1)$$

where H, T, T_d, and U_z represent the PBL height (m), surface air temperature (K), surface dew point (K), and mean wind speed ($m\,s^{-1}$) at height of Z ($Z = 10$ m), respectively. f and z_0 are the Coriolis parameter (s^{-1}) and surface roughness length (0.5 m in this study), respectively. P is the Pasquill stability level, classified as six categories from very unstable (A), moderately unstable (B), slightly unstable (C), neutral (D), slightly stable (E) to moderately stable (F) (Pasquill, 1961). To relate RH with the PBL height, we adopted a modified Nozaki's equation using $(100-RH)/5$ to replace $(T-T_d)$ according to Wallace and Hobbs (2005) and Tie et al. (2017). The measured wind speeds were used in the calculations. For the severe haze events, the atmosphere was stable, and the Pasquill stability levels were set as 4–5. The inputs of the PBL height for the clean and aged-BC cases were based on ceilometer measurements, showing that the PBL height increased by about 700–900 m from the aged-BC to the clean cases.

3 Results and discussion

3.1 Regional characteristics of severe haze episodes

Measurements of the $PM_{2.5}$ mass concentrations from 25 September to 14 November 2013 reveal that severe haze occurs frequently over the NCP, reflected by a periodic cycle of 4–7 d with highly elevated PM pollution (Fig. 1a–c). Each severe haze episode consists of a clean period, a transition period from clean to hazy conditions, and a polluted period with very high PM levels. For the three megacities across the NCP, i.e., Beijing, Baoding, and Shijiazhuang, the maximal mass concentration of $PM_{2.5}$ consistently exceed several hundred micrograms per cubic meter during the polluted period. The $PM_{2.5}$ concentrations at the three megacities exhibit a remarkable similarity in the timing and magnitude for the peak $PM_{2.5}$ concentrations. The nearly synchronized temporal variations in the PM levels among the three megacities indicate a prominent characteristic of severe haze formation, indicating the importance of in situ PM production over the entire region. During the evolution from clean, transition, to polluted periods, the RH and wind speed are consistently increased and decreased, respectively (Fig. 1d).

The two polluted events on 28 September (EP1) and 5 October (EP2) are captured from both in situ measurements (Fig. 1) and satellite observations (Fig. 2). The satellite MODIS data illustrate that the maximal AOD area occurs in the three megacities (i.e., BJ, BD, and SJZ). For example, the AOD value in Beijing exceeds 4.0 and 2.0, during EP1 and EP2, respectively. The spatial distribution of severe regional haze events is also depicted from the satellite visible images, showing that a grey haze plume covers a substantial portion of the NCP region (Fig. 2c and d). The coincidence of the highest AOD areas with the locations of the megacities is also discernable from the mean AOD values averaged over all the hazy days (e.g., daily $PM_{2.5} > 200\,\mu g\,m^{-3}$) in 2013 (Fig. S3 in the Supplement), showing a large zone of elevated AOD values over the three megacities. In contrast, the fall seasonal and annual AOD means averaged over all days in 2013 show that the maximal AOD values are located to the south of Beijing (Fig. 2e and f), reflecting the typical regional transport patterns over this region (Guo et al., 2014; An et al., 2019; Peng et al., 2021). In addition, the occurrence of severe haze events is consistently accompanied by stagnant weather, characterized by weak southerly winds in Beijing and its surrounding areas (Fig. 2a and b). For example, the wind speed is typically less than $1\,m\,s^{-1}$ in the highest AOD area (Fig. 2a and b), compared to that of a few to $10\,m\,s^{-1}$ during the clean period (Fig. 1d). Air stagnation retards PM dispersion, resulting in minimal regional transport during the polluted period. On the other hand, the gaseous aerosol precursors (e.g., SO_2, NO_x, VOCs, and NH_3 with the chemical lifetimes from hours to days) are sufficiently transported and dispersed prior to haze development over this region, as evident from much higher wind speeds during the clean period (Fig. 1d). Efficient regional transport of the gaseous aerosol precursors explains the similarity in the spatial/temporal PM variations, since well-mixed gaseous aerosol precursors result in similar in situ PM production under stagnant conditions (Fig. 1a–c). Moreover, the coincidence of the AOD hotspots with the three megacities (Figs. 2a, b and S3) indicates more efficient in situ PM production over the megac-

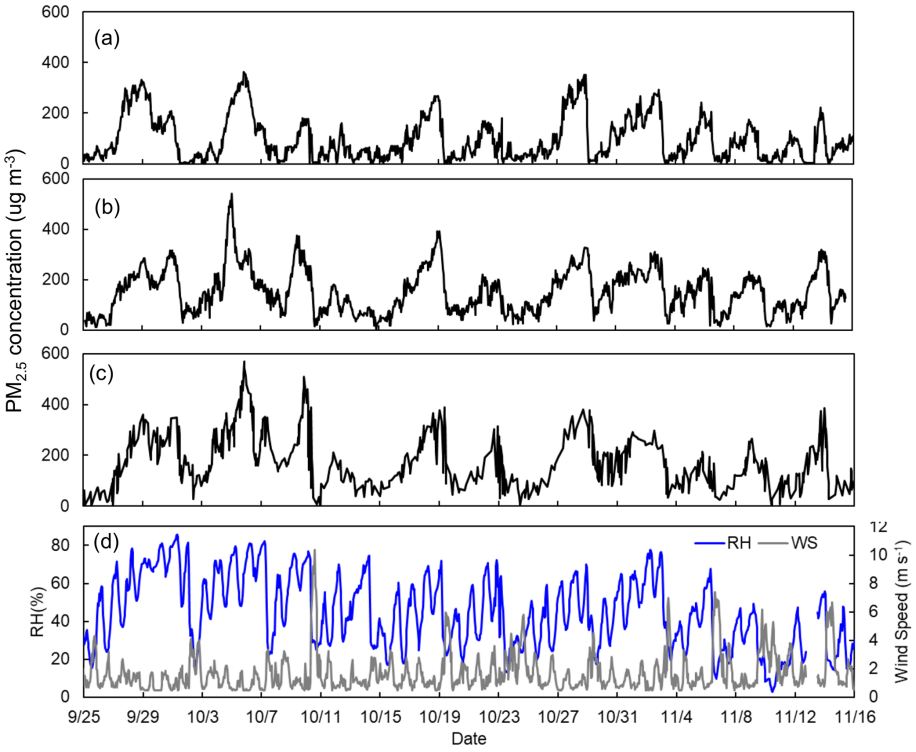

Figure 1. Time series of $PM_{2.5}$ mass concentration measured at three megacities over the North China Plain (NCP), including **(a)** Beijing, **(b)** Baoding, and **(c)** Shijiazhuang from 25 September to 16 November 2013, and **(d)** the associated relative humidity (RH, blue line) and 10 m wind speed (grey line) in Beijing. The $PM_{2.5}$ mass concentration and meteorological fields in Beijing are taken from Guo et al. (2014), and the $PM_{2.5}$ data for Baoding and Shijiazhuang are taken from https://air.cnemc.cn:18007/ (last access: 12 January 2021). Two severe haze episodes from 25–29 September and from 2–7 October are selected as the case studies in this work, and the two vertical dash lines label the time for the peak $PM_{2.5}$ concentration in Beijing.

ities, suggesting a key role of traffic emissions (i.e., anthropogenic VOCs and NO_x) in facilitating regional severe haze formation. While wind fluctuation likely results in PM variation in an isolated location, especially for Beijing, which is situated at the northern edge of the NCP (Li et al., 2015), our analysis of temporal/spatial PM distributions indicates that the dominant regional features during the polluted period are reflected by rapid in situ PM production and inefficient transport, both of which are amplified by air stabilization.

3.2 Photochemical PM formation

To further elucidate the role of in situ photochemical production in haze development, we analyzed the temporally resolved PM properties in Beijing. Typically, haze evolution in this region involves new particle formation and subsequently growth of nucleation mode particles during the clean period, which are mainly driven by photochemistry (Lee et al., 2019; Guo et al., 2020). Evidently, the $PM_{2.5}$ mass concentration increases by more than $200\,\mu g\,m^{-3}$ in less than 8 h during the transition period for EP1 and EP2 (Fig. 3a and b), which is dominated by the increase in the SOA mass concentration linked to photochemical oxidation of VOCs (Guo et al., 2014; Liu et al., 2021). The mass concentration of OOA is typically considered as a surrogate for SOA (Wood et al., 2010). Since OOA and the level of oxidants, O_x ($[O_x] \equiv [O_3] + [NO_2]$), are both produced from oxidation of VOCs (Suh et al., 2001; Fan and Zhang, 2004; Zhao et al., 2004, 2005; Ji et al., 2017) and have a lifetime of longer than 12 h, it is anticipated that both quantities are correlated, when their formations occur on a similar timescale and at the same location (Atkinson, 2000). Figure 3a–d show that the increase in OOA is well correlated with the O_x level during the transition period. The R^2 from linear regression between OOA and O_x during the transition period (i.e., from 07:00 am to 02:30 pm) is 0.96 for EP1 and 0.95 for EP2 (Fig. 3e). The high correlation between OOA and O_x implies important in situ production of PM via photochemical reactions, consistent with the ground-based measurements (Fig. 1) and satellite observations for PM (Figs. 2 and S3). The mean ratio of [OOA] to $[O_x]$ for the two episodes in Beijing is 0.34 ($\mu g\,m^{-3}\,ppb^{-1}$), suggesting highly efficient photochemistry. For comparison, the mean ratio of [OOA] to $[O_x]$ during the two episodes in Beijing is about 2.4 and 5.1 times of those in Mexico City and Houston (Wood et al., 2010), respectively, indicating that the photochemical PM formation in Beijing

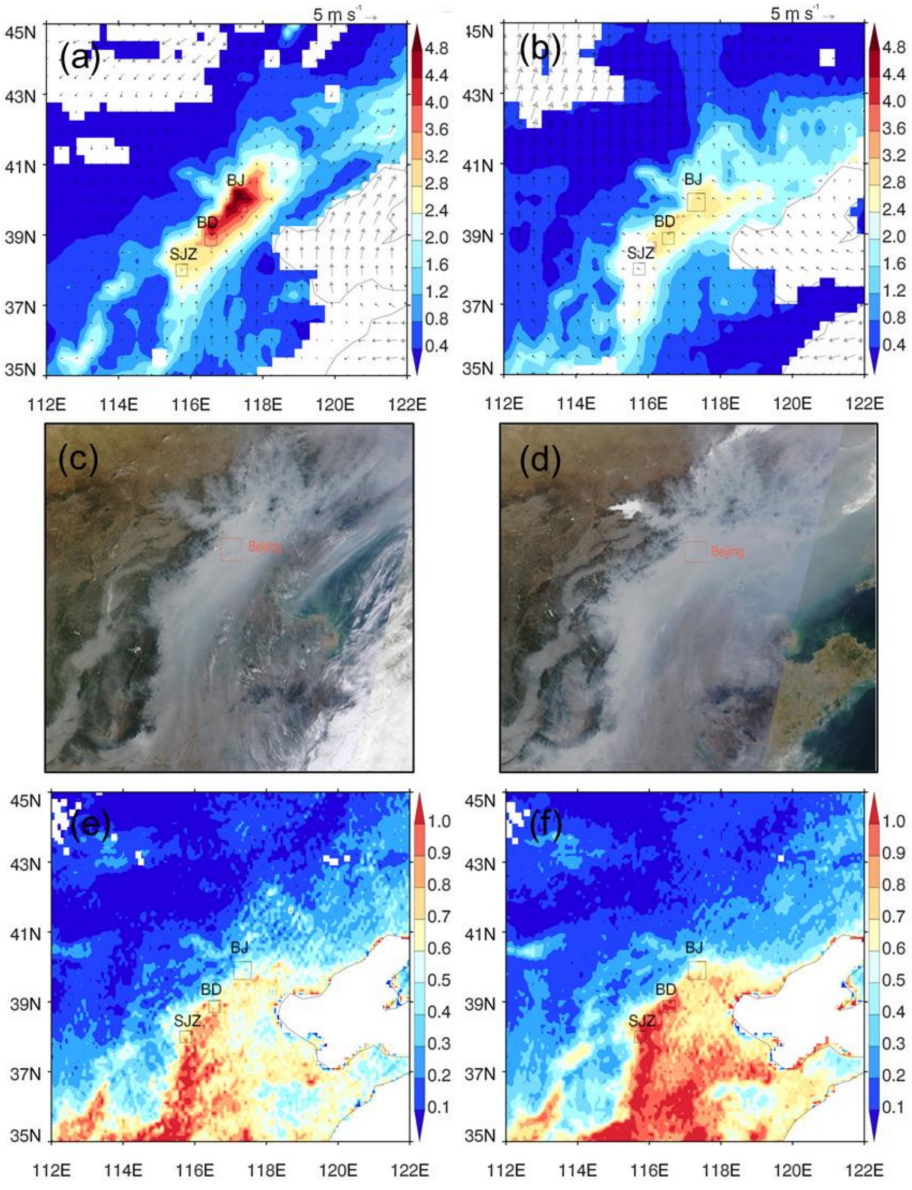

Figure 2. MODIS AOD **(a, b)** and visible images **(c, d)** illustrating the two severe haze episodes in Fig. 1. Panels **(a)** and **(c)** correspond to 28 September, 2013, and **(b)** and **(d)** correspond to 5 October 2013. Panels **(e)** and **(f)** represent MODIS AOD of fall seasonal and annual mean in 2013. The megacities of Beijing (BJ), Baoding (BD), and Shijiazhuang (SJZ) are marked as squares. Wind field imposed on **(a)** and **(b)** is based on ECMWF reanalysis data.

is much more efficient than those in Mexico City and Houston (Fig. 3f). The more efficient photochemical formation of PM in Beijing is attributable to the presence of higher levels of anthropogenic aerosol precursors, such as anthropogenic VOCs and NO_x, than those in the other two cities (Guo et al., 2014; Zhang et al., 2015b). On the other hand, the correlation between [OOA] and [O_x] exists only during the transition stage but vanishes during the polluted period. The latter is evident from the continuing increase in [OOA] but decreasing [O_x]. In particular, O_3 production is significantly suppressed during the polluted periods because of reduced solar ultraviolet radiation, leading to inefficient photooxidation (Wu et al., 2020; Peng et al., 2021). Several previous studies have attributed highly elevated levels of $PM_{2.5}$ during the polluted period to the importance of multiphase chemistry to contribute to SIA and SOA formation (G. Wang et al., 2016; An et al., 2019; Peng et al., 2021). For example, sulfate formation is effectively catalyzed by BC (Zhang et al., 2020) and considerably enhanced via aqueous oxidation of SO_2 by NO_2 in the presence of NH_3 during the transition/polluted periods (G. Wang et al., 2016), both increasing with increasing RH. Also, oligomerization from dicarbonyls increases at

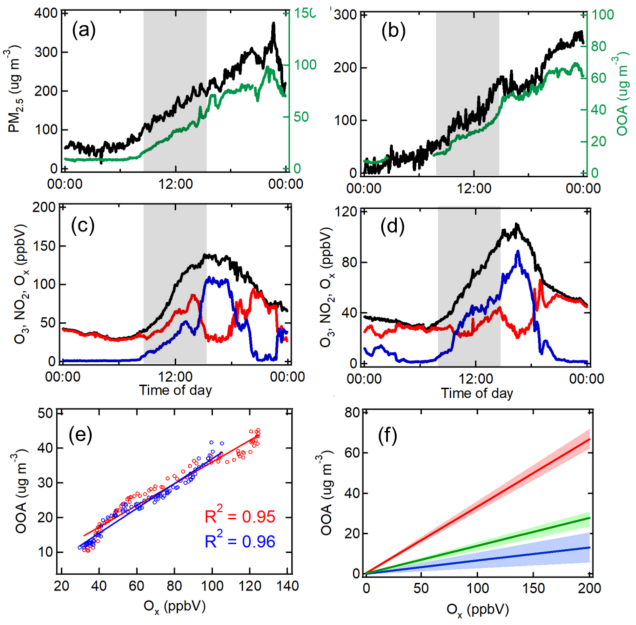

Figure 3. Temporal evolutions of measured $PM_{2.5}$ (black) and OOA (green) mass concentrations **(a, b)** and O_3 (blue), NO_2 (red), and O_x (black) mixing ratios **(c, d)** during the early stages of the two haze episodes. Panels **(a)** and **(c)** are for the episode starting on 27 September 2013, and **(b)** and **(d)** are for the episode starting on 4 October 2013. Panel **(e)** represents linear regression between O_x and OOA on 27 September (red circles) and 4 October (blue circles) 2013. The grey shadings **(a–d)** correspond to the largest variation in O_x, which covers both the clean and transition periods. Panel **(f)** corresponds to the ratios of [OOA] changes to [O_x] changes (Δ[OOA]/Δ[O_x]) for Beijing (red), Mexico City (green), and Houston (blue). The ratios for Beijing are derived from this study, and the ratios for Mexico City and Houston taken from Wood et al. (2010). Color shadings in **(f)** represent the range between the minimum and maximum ratios.

high RH (Li et al., 2021a, b), contributing to significantly enhanced SOA formation during the polluted periods (Zhang et al., 2021).

Note that both the photochemical production and PBL evolution contribute to PM accumulation at the ground level, since the PBL development leads to vertical ventilation and dilution during the daytime. The ceilometer-retrieved PBL height increases about 200 m (150 m) from morning to afternoon and decreases by about 150 m (400 m) from afternoon to midnight on 27 September (4 October) (Fig. S4 in the Supplement). Clearly, the largest PM increase and the strong correlation between OOA and O_x during the morning and early afternoon hours indicate that the photochemical production dominates the PM increase during the transition period.

3.3 Impacts of the haze–PBL interaction

3.3.1 A positive feedback of PM accumulation

To assess the impacts of haze–PBL interactions on PM pollution, we evaluated the correlation between the PM level and PBL height. Figure 4 shows an analysis of daily PBL height versus $PM_{2.5}$ concentration between clean and hazy days from the ground-based measurements and the MERRA2 reanalysis data in 2013. The daily PBL height is negatively correlated with surface $PM_{2.5}$ concentration (Fig. 4a). The diurnal cycle of the PBL height shows that the PBL height on severe haze days (daily $PM_{2.5}$ concentration $> 200\,\mu g\,m^{-3}$) is significantly lower than that on clean days (daily $PM_{2.5}$ concentration $< 30\,\mu g\,m^{-3}$), with a maximum difference of 800 m (Fig. 4b). Furthermore, the dimming area over the NCP, which is reflected by the lower mean of the satellite-retrieved surface solar radiation (SSR) averaged over all the severe haze days in 2013, coincides with the region with the highest AOD (Fig. S3), implying a strong spatial association between the solar radiation intensity and PM pollution at the surface. The co-locations in the areas between the lowest SSR and highest AOD also reflect the occurrence of the highest PM levels at the megacities during the regional severe haze episodes.

We further elucidated the response of PBL development to the PM pollution, and the linkage between the aerosol–PBL interactions and aerosol radiative effects are further elucidated by performing sensitivity modeling studies on the 2 hazy days (Figs. 5 and 6). The performance of the model simulations was validated by comparison with field observations. The simulated temperature and RH are consistent with the sounding data in light of the vertical variations (Fig. S2 in the Supplement). The simulated AOD at 550 nm is 0.05 and 3.6 on 25 and 28 September 2013 for EP1, respectively, and 0.04 and 2.0 on 2 and 5 October 2013 for EP2, respectively, in qualitative agreement with the Aerosol Robotic Network (AERONET) measurements in Beijing (Table 2). The simulated 1-day accumulated surface solar radiation and the peak solar radiation flux in the aged-BC case for EP1 (EP2) are $9.2\,MJ\,m^{-2}$ ($11.3\,MJ\,m^{-2}$) and $326\,W\,m^{-2}$ ($402\,W\,m^{-2}$), respectively, comparable to the ground-based measurement of $10.6\,MJ\,m^{-2}$ ($9.8\,MJ\,m^{-2}$) and $408\,W\,m^{-2}$ ($452\,W\,m^{-2}$) in Table 2. The temporal evolutions of PBL and its peak heights derived from the aged-BC cases are also consistent with the available measurements (Fig. 5a and g).

The simulated maximal height of PBL under the polluted condition is reduced by more than 300 m relative to the clean condition (Fig. 5a and g). The reduction in PBL height is explained by the aerosol radiative effects. Under the polluted condition, a warmer temperature is located at the altitude of around 1.2 km, and less SSR reaches the ground level (Fig. 5e and k, f and l). Also, the surface temperature is reduced by several degrees (Fig. 5e and k, and Fig. 6a and c). The extents of warming in the upper boundary layer and cooling at the

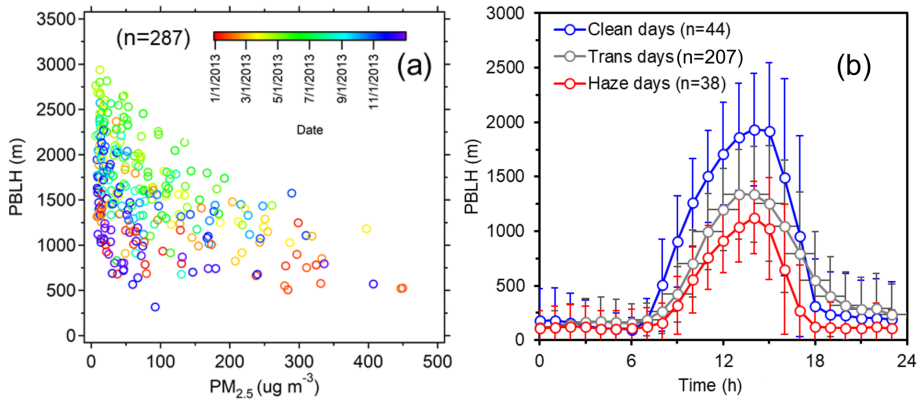

Figure 4. **(a)** Scatterplot for daily mean PBL height versus $PM_{2.5}$ concentration and **(b)** mean diurnal variations of PBL height averaged over clean days (daily mean $PM_{2.5} < 30\,\mu g\,m^{-3}$), extremely hazy days (daily mean $PM_{2.5} > 200\,\mu g\,m^{-3}$), and transition days ($30\,\mu g\,m^{-3} <$ daily mean $PM_{2.5} < 200\,\mu g\,m^{-3}$) in 2013 in Beijing, China. *n* denotes the number of days used for plotting. The vertical lines in **(b)** denote ± 1 standard deviation. All the precipitation days were filtered out.

Table 2. Comparisons between measurements and simulations for aerosol optical properties and surface solar radiation during the two haze episodes (EP1/EP2).

Case	SSA	AOD	Max solar radiation flux at surface ($W\,m^{-2}$)	Accumulated surface solar radiation ($MJ\,m^{-2}$)
$E_{MAC\text{-}BC} = 2.4$	0.83/0.83	3.7/2.1	342/403	10.1/11.5
Aged-BC	0.87/0.87	3.6/2.0	326/402	9.2/11.3
Observations	0.90[a]	3.5/2.4[b]	480[c]/452	10.6[c]/9.8

[a] SSA is based on a recent field campaign conducted in 2015 in Beijing. [b] AOD is based on AERONET measurements at the Beijing site (http://aeronet.gsfc.nasa.gov/, last access: 21 January 2021). [c] The maximum solar radiation flux and accumulated surface solar radiation were measured at China Meteorological Research Institute, Beijing, China.

surface due to the aerosol effect in this study are consistent with the observational analysis on North China by Huang et al. (2018), indicating that our simulations well reproduce the aerosol radiative effect under severe regional haze condition. Consequently, the turbulent kinetic energy (TKE) is reduced, and the updraft is weakened in the aged-BC cases relative to the clean cases (Fig. 5b, c, h and i), leading to an enhanced atmospheric stratification and hindered development of PBL. The largely reduced TKE during the polluted periods from the model simulations is consistent with field measurements, showing that the turbulent fluxes are greatly reduced in the mixed surface layer under polluted conditions (Wilcox et al., 2016). In addition, surface winds are reduced by $0.7\,m\,s^{-1}$ from clean to aged-BC cases (Fig. 6b and d), leading to suppressed entrainment aloft and restricted development of the PBL.

The interaction between aerosols and PBL induces further feedbacks at the surface by altering atmospheric dynamic/thermodynamic conditions and stability. For example, the PM concentration at the ground level accumulates when the PBL is compressed, resulting in a smaller extent for vertical dilution. Also, the diurnal feature of PM pollution diminishes because of collapsed PBL, allowing PM to continuously accumulate at the surface. In addition, horizontal advection is also suppressed under polluted conditions, as reflected by weak wind speeds. Consequently, the heavy haze period persists over an extensive period (about 4–7 d) over this region and is only dissipated by strongly northerly winds associated with frontal passage (Guo et al., 2014; An et al., 2019). The continuous PM accumulation for multiple days over the NCP is distinct from other megacities across the world, such as Houston, Los Angeles, and Mexico City, which always exhibit a clear diurnal feature of the PM levels (Zhang et al., 2015b), implying a key role of the haze–PBL interaction in deteriorating air quality and worsening the hazy condition in this region. The significant aerosol–PBL interaction and the impact on surface air pollution revealed in our simulation studies are also evident in multiple observation-based studies in China (Dong et al., 2017; Huang et al., 2018; Su et al., 2020). However, there might exist certain uncertainties in evaluating the aerosol impacts on PBL development based on the simulation experiments. Previous observational analysis (Dong et al., 2017; Su et al., 2020) suggested that the aerosol–PBL interaction also varies with the aerosol vertical structure, compared to an exponential decreasing aerosol profile assumed in our simulations.

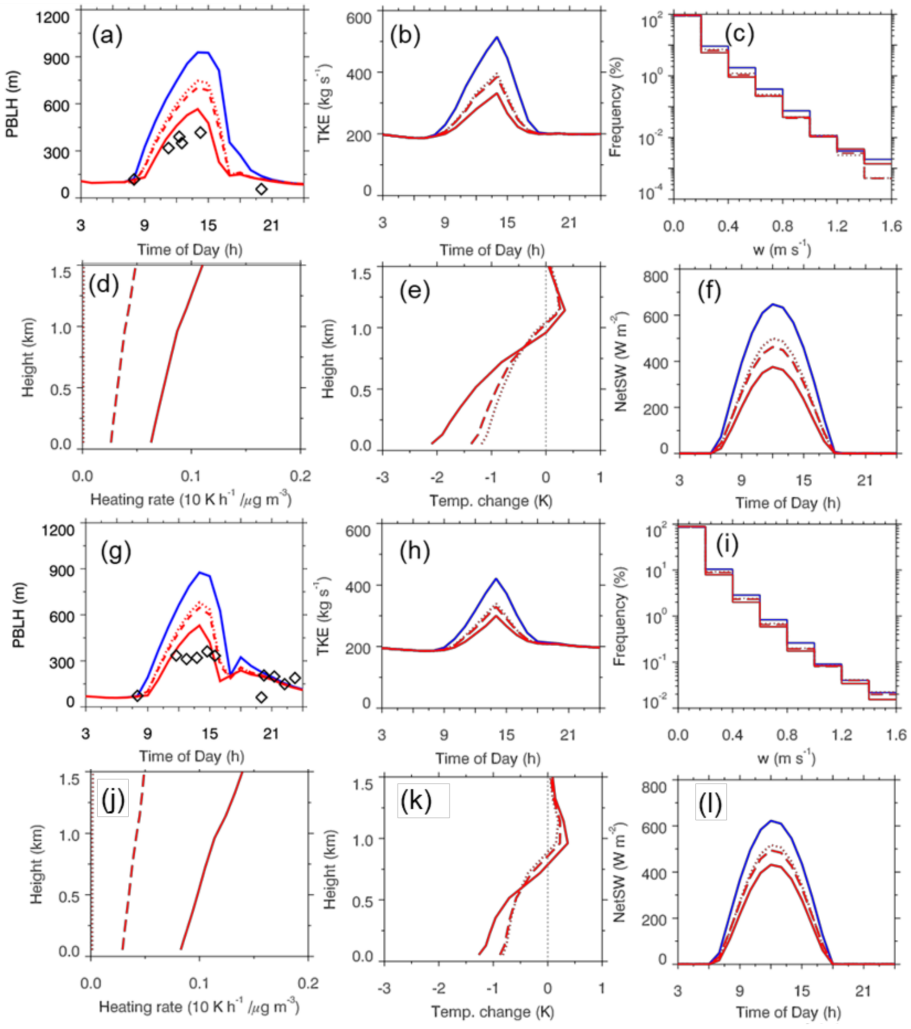

Figure 5. Simulated meteorological conditions and thermodynamic and dynamic feedbacks under the clean conditions (blue solid) and the polluted conditions for the non-BC (red dot), fresh-BC (red dashed), and aged-BC (red solid) cases. Panels **(a)** and **(g)** correspond to simulated diurnal variations of PBL height, **(b)** and **(h)** correspond to the diurnal variations of vertically integrated TKE, and **(c)** and **(i)** represent the frequency distribution of updraft. Panels **(d)** and **(j)** are the vertical profile of the shortwave heating rate per unit aerosol mass for the non-BC (red dot line), fresh-BC (red dash line), and aged-BC (red solid line) cases. Panels **(e)** and **(k)** are similar to **(d)** and **(j)** but for the temperature changes. Panels **(f)** and **(l)** are diurnal evolutions of net surface shortwave radiation (NetSW). Panels **(a–f)** are for EP1 and **(g–n)** are for EP2. The black hollow squares in **(a)** and **(g)** denote measurements of PBL height from ceilometer.

The suppression in PBL height results in significant enhancement of atmospheric moisture, another crucial factor affecting the haze evolution, which promotes the occurrence of multiphase reactions (Li et al., 2021a, b). The measured RH increases greatly during the two episodes (Fig. 1d), i.e., from about 18 %–19 % on the clean days (25 September and 2 October) to 53 %–55 % on the polluted days (28 September and 5 October). To evaluate the sensitivity of the atmospheric moisture to the PBL height, we employed a modified Nozaki equation (Nozaki, 1973; Tie et al., 2017) to calculate the RH under different PBL height scenarios using the observed meteorological conditions as inputs (Table 3). The calculated RH increases from 29 % to 68 % for EP1 and from 28 % to 73 % for EP2, when the PBL height decreases from 1180 to 395 m and 1313 to 370 m from clean to polluted days for EP1 and EP2, respectively, indicating that the humidity is highly sensitive to the PBL height.

The elevated RH during the polluted period is explained from collapsed PBL to inhibit vertical moisture transport, reduced surface temperature leading to lower saturation vapor pressure, and inefficient entrainment of dry air aloft (Fan et al., 2008; Liu et al., 2013). In addition, enhanced moisture leads to hygroscopic growth of aerosol particles (Liu et al., 2013; Tie et al., 2017). For example, the growth hygroscopic factor relevant to the RH enhancement during EP1 and EP2 increases from 1.3 on the clean days to 1.5 on the

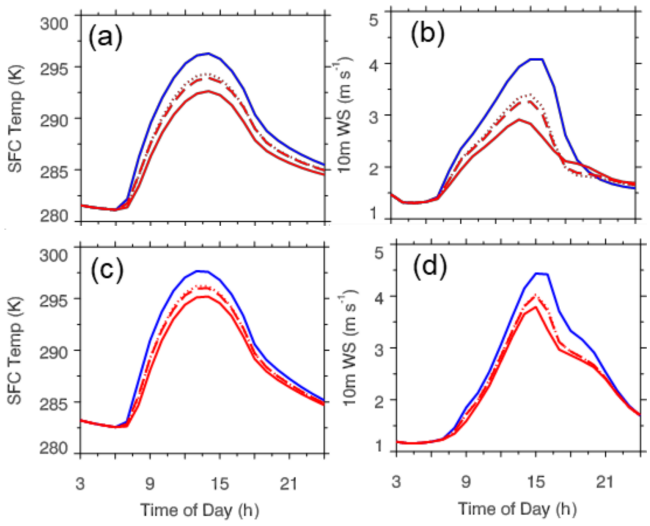

Figure 6. Temporal evolutions of surface temperatures **(a, c)** and 10 m wind speeds **(b, d)** under the clean conditions (blue solid) and the polluted conditions for the non-BC (red dot), fresh-BC (red dashed), and aged-BC (red solid) cases. Panels **(a)** and **(b)** correspond to EP1, and **(c)** and **(d)** correspond to EP2.

Table 3. RH sensitivity to PBL height changes calculated using the empirical equations by Tie et al. (2017). PBL heights are from ceilometer measurements.

	Condition	Mixing layer height (m)	RH	Difference in RH (Clean – Hazy)
EP1	Hazy	395	68 %	39 %
	Clean	1180	29 %	
EP2	Hazy	370	73 %	45 %
	Clean	1313	28 %	

hazy days, using an empirical equation derived according to Meier et al. (2009). The additional aerosol growth causes additional attenuation of incoming solar radiation by scattering and absorption to amplify PBL suppression. Moreover, an enlarged aerosol surface area (due to hygroscopic growth) and elevated RH during the polluted periods favor aqueous-phase reactions to produce sulfate, nitrate, and SOA (G. Wang et al., 2016). For example, a recent experimental/-field study has shown enhanced sulfate formation, which is catalyzed by BC and increases monotonically from 10 % to 70 % RH (Zhang et al., 2020). Also, the aqueous reaction of dicarbonyls, which are produced with high yields from oxidation of aromatic VOCs, is significantly enhanced at high RH to yield oligemic products and enhance SOA formation (Li et al., 2021a, b). Hence, enhanced PM production near the ground level strengthens the suppressing effect for the PBL development and results in stabilization and moisture enhancement, constituting positive feedback to amplify the haze development.

3.3.2 The BC effects

We performed model sensitivity simulations to elucidate the role of BC in PBL suppression by considering the non-BC, fresh-BC, and aged-BC scenarios during the polluted periods. Comparison shows a negligible effect on the haze–PBL interaction between the non-BC and fresh-BC cases (Figs. 5, 6 and S5 in the Supplement) but large changes in solar radiation and thermodynamic/dynamic conditions within the PBL between the non-BC/fresh-BC and aged-BC cases, which are attributed to the radiative effects of aged BC. For example, the shortwave heating rate per unit mass is much larger for aged-BC than non-BC and is 2 times higher for aged-BC than fresh-BC (Fig. 5d and j), suggesting that the BC aging process greatly attenuates incoming solar radiation. Although BC accounts for only 6 % of the total aerosol mass under the polluted conditions, about one-third of the total reduction in SSR for full-component aerosols is attributed to absorption enhancement after BC aging (Fig. 5f and l). The reduced SSR by the BC aging leads to a cooling of 0.5–0.8 K at the surface. As a result, BC aging contributes significantly to atmospheric stabilization, as evident from weaker updrafts, smaller TKE, and shallower PBL for the aged-BC case (Fig. 5).

The BC aging causes a decrease in the maximum PBL height (at noontime) by about 150 m for the aged-BC case compared to the non-BC and fresh-BC cases. Overall, the BC aging contributes more than 30 % of the total reduction in the PBL height by all aerosol components. The restricted PBL development by BC absorption in our work is consistent with that identified previously (Ding et al., 2016; Petäjä et al., 2016). Using a radiative transfer model, Zhang et al. (2020) show large strongly positive radiative forcing in the atmosphere and strongly negative radiative forcing at the surface by BC aging, consistent with those of the maximal estimates at about noontime from our calculations (Fig. 5i and f). The significant role of BC in atmospheric heating is consistent with long-term observations (Huang et al., 2018), showing that heating in the atmosphere is mainly caused by absorbing aerosols such as BC.

3.4 Aerosol direct radiative forcing

The aerosol direct radiative forcing during regional haze also exhibits a profound climatic effect (Ramanathan et al., 2007). Figure 7 shows that the total aerosol radiative forcing at the surface (SFC) and in the atmosphere (ATM) during the haze episodes EP1 (EP2) are −87.8 (−62.8) $W m^{-2}$ and 82.2 (56.9) $W m^{-2}$, respectively. The positive radiative forcing by all aerosols in the atmosphere is dominated by that of aged BC, which accounts for 80 % of the total radiative forcing for both episodes. The net radiative forcing at the top of the atmosphere (TOA) by all aerosols for EP1 (EP2) is around −5.6 (−5.9) $W m^{-2}$, much smaller than the non-BC case with a large negative value of −36.8 (−26.0) $W m^{-2}$. The strong cooling at the surface is largely

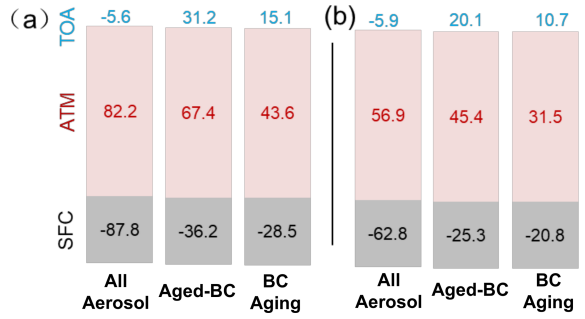

Figure 7. Aerosol direct radiative forcing for total aerosol (left column), aged-BC (middle column), and BC aging (right column) on the top of the atmosphere (TOA), in the atmosphere (ATM), and at the surface (SFC) for 2 severe haze days in Beijing. Panels **(a)** and **(b)** correspond to EP1 and EP2, respectively. The forcing caused by BC aging corresponds to the difference in the simulations between the fresh-BC and aged-BC cases. The number denotes radiative forcing in the unit of $W\,m^{-2}$.

canceled out by the strong warming in the atmosphere under the polluted condition, leading to a small net TOA forcing. Clearly, BC aging contributes significantly to cooling at the surface and warming aloft and, hence, the overall radiative budget during the polluted periods. Climatologically, the aerosol TOA forcing on the regional/national level has been shown to be nearly zero or slightly positive in China (Li et al., 2007; Ramanathan et al., 2007; Ding et al., 2016), also demonstrating that the large positive forcing by absorbing aerosols greatly compensates the negative forcing by the non-absorbing aerosols (Table S1 in the Supplement). Therefore, regional global warming is likely mitigated by reducing BC emissions (Z. L. Wang et al., 2015).

4 Conclusions

In this work, we analyzed the temporal and spatial characteristics of PM pollution during severe haze events over the NCP, by examining ground-based measurements and satellite observations. Severe haze occurs frequently over this region, evident from a periodic (4–7 d) cycle of highly elevated PM pollution. The PM evolutions among the three megacities (Beijing, Baoding and Shijiazhuang) exhibit a remarkable similarity during the haze events, showing nearly synchronized temporal variations in the PM levels. The similar timing and magnitude in the peak $PM_{2.5}$ concentrations among the three megacities indicate significant in situ PM production. Satellite measurements show that the AOD hotspots during the polluted period are co-located with the three megacities, but they are distinct from seasonal and annual AOD means, indicating the importance of urban emissions (mainly traffic emissions consisting of anthropogenic VOCs and NO_x). In situ PM production occurs most efficiently over the megacities, and urban sources relevant to traffic emissions play a critical role in regional severe haze formation.

Our result reveals that the rapid photochemistry drives the PM production during the transition period. There exist concurrent increases in OOA and $PM_{2.5}$ concentrations and a strong correlation between OOA and O_x concentrations during this period. The $[OOA]/[O_x]$ ratio in Beijing is much higher than that in Mexico City and Houston, attributable to much higher level of gaseous precursors (i.e., anthropogenic VOCs and NO_x) in Beijing than the other two cities. The correlation between [OOA] and $[O_x]$, however, vanishes during the polluted period, when O_3 production is significantly suppressed because of reduced solar ultraviolet radiation and inefficient photooxidation (Wu et al., 2020; Peng et al., 2021). The continuing increases in $PM_{2.5}$ and OOA with decreasing O_x during the polluted period imply a key role of multiphase chemistry in driving the haze severity, when the RH level is significantly elevated. The continuous growth in $PM_{2.5}$ and OOA during the polluted period has been explained by an increasing importance of heterogeneous chemistry to contribute to sulfate, nitrate, and SOA formation (G. Wang et al., 2016; An et al., 2019; Peng et al., 2021; Zhang et al., 2021).

Using the WRF model coupled with an explicit aerosol radiative module, we elucidated the underlying mechanism relevant to the haze–PBL interactions, showing a positive feedback to haze formation at the ground level. The PBL height is largely reduced under the polluted condition, since the PBL is markedly suppressed (as indicated by the reduced TKE and weakened updraft), because of strong aerosol heating in the atmosphere and strong cooling at the surface. The PM concentration near the surface accumulates significantly in a compressed PBL, since PM dispersion is unfavorable in the stratified and collapsed PBL, leading to continuous growth and accumulation of PM over multiple days. Calculations using the modified Nozaki's equation show that the suppressed PBL results in a great enhancement of atmospheric moisture near the surface. A more humid condition leads to hygroscopic growth of aerosol particles and more efficient multiphase PM production. Therefore, haze development near the surface is considerably exacerbated because of the positive feedback in responding to the atmospheric moisture and thermodynamic/dynamic conditions to amplify the haze severity.

Our combined observational analysis of the temporal/spatial PM distributions and modeling unravel a dominant regional characteristic for severe haze evolution in the NCP region, showing rapid in situ PM production and inefficient transport, both of which are amplified by air stabilization. On the other hand, regional transport sufficiently disperses the gaseous aerosol precursors (SO_2, NO_x, VOCs, and NH_3) during the clean period, which subsequently result in rapid in situ PM production via photochemistry during the transition period and via multiphase chemistry during the polluted period.

The modeling simulations on two haze episodes indicate important regional climatic effects. The net TOA forcing for the 2 hazy days is about -5.6 to $-5.9\,W\,m^{-2}$, showing strong negative radiative forcing (cooling) of -63 to $-88\,W\,m^{-2}$ at the surface and strong positive radiative forcing (warming) of 57 to $82\,W\,m^{-2}$ in the atmosphere. BC represents the dominant contributor to the positive aerosol radiative forcing in the atmosphere, thus playing a significant role in the haze–PBL interaction. Specifically, BC aging contributes to more than 30 % of the PBL collapse induced by total aerosols and about 50 % of the TOA positive radiative forcing. Our work highlights the necessity to better understand the BC aging process and improve representation in atmospheric models for accurate assessment of the aerosol climatic effects. We conclude that reduction in BC emissions achieves co-benefits, which improve local and regional air quality by minimizing air stagnation and mitigate the global warming by alleviating the positive direct radiative forcing.

Code and data availability. The source code of WRF was similar to that described previously by Li et al. (2008) and Fan et al. (2008). All data employed in the present study were described in Sect. 2.1 and are also available from the author (Yun Lin) upon request.

Supplement. The supplement related to this article is available online at: https://doi.org/10.5194/acp-22-4951-2022-supplement.

Author contributions. RZ created the original research framework and provided research direction. YL and YW developed the model theory, co-wrote the software, established a database, and created the figures. All authors analyzed the data and co-wrote the manuscript. BP, JH, SG, HM, MZ, and MGH analyzed the PM data; PT provided and processed observed meteorology data; QS, YJ, and JZ provided feedback and contributed to the draft of the manuscript.

Competing interests. The contact author has declared that neither they nor their co-authors have any competing interests.

Disclaimer. Publisher's note: Copernicus Publications remains neutral with regard to jurisdictional claims in published maps and institutional affiliations.

Acknowledgements. The modeling portion of this research was conducted at the TAMU High Performance Research Computing. We thank Hong-Bin Chen and Philippe Goloub for the data at the Beijing AERONET site.

Financial support. This research has been supported by a collaborative program between Texas A&M University (TAMU) and the Natural Science Foundation of China (NSFC).

Review statement. This paper was edited by Zhanqing Li and reviewed by three anonymous referees.

References

Aiken, A. C., Salcedo, D., Cubison, M. J., Huffman, J. A., DeCarlo, P. F., Ulbrich, I. M., Docherty, K. S., Sueper, D., Kimmel, J. R., Worsnop, D. R., Trimborn, A., Northway, M., Stone, E. A., Schauer, J. J., Volkamer, R. M., Fortner, E., de Foy, B., Wang, J., Laskin, A., Shutthanandan, V., Zheng, J., Zhang, R., Gaffney, J., Marley, N. A., Paredes-Miranda, G., Arnott, W. P., Molina, L. T., Sosa, G., and Jimenez, J. L.: Mexico City aerosol analysis during MILAGRO using high resolution aerosol mass spectrometry at the urban supersite (T0) – Part 1: Fine particle composition and organic source apportionment, Atmos. Chem. Phys., 9, 6633–6653, https://doi.org/10.5194/acp-9-6633-2009, 2009.

An, Z. S., Huang, R. J., Zhang, R. Y., Tie, X. X., Li, G. H., Cao, J. J., Zhou, W. J., Shi, Z. G., Han, Y. M., Gu, Z. L., and Ji, Y. M.: Severe haze in northern China: A synergy of anthropogenic emissions and atmospheric processes, P. Natl. Acad. Sci. USA, 116, 8657–8666, https://doi.org/10.1073/pnas.1900125116, 2019.

Atkinson, R.: Atmospheric chemistry of VOCs and NO_x, Atmos. Environ., 34, 2063–2101, https://doi.org/10.1016/S1352-2310(99)00460-4, 2000.

Bond, T. C., Doherty, S. J., Fahey, D. W., Forster, P. M., Berntsen, T., DeAngelo, B. J., Flanner, M. G., Ghan, S., Kärcher, B., Koch, D., Kinne, S., Kondo, Y., Quinn, P. K., Sarofim, M. C., Schultz, M. G., Schulz, M., Venkataraman, C., Zhang, H., Zhang, S., Bellouin, N., Guttikunda, S. K., Hopke, P. K., Jacobson, M. Z., Kaiser, J. W., Klimont, Z., Lohmann, U., Schwarz, J. P., Shindell, D., Storelvmo, T., Warren, S. G., and Zender, C. S.: Bounding the role of black carbon in the climate system: A scientific assessment, J. Geophys. Res.-Atmos., 118, 5380–5552, https://doi.org/10.1002/jgrd.50171, 2013.

Bouarar, I., Wang, X. M., and Brasseur, G. P.: Air Pollution in Eastern Asia: An Integrated Perspective Preface, ISSI Sci. Rep. Ser., 16, V–Viii, https://doi.org/10.1007/978-3-319-59489-7, 2017.

Cai, W., Li, K., Liao, H., Wang, H., and Wu, L.: Weather conditions conducive to Beijing severe haze more frequent under climate change, Nat. Clim. Change, 7, 257, https://doi.org/10.1038/nclimate3249, 2017.

Che, H., Xia, X., Zhu, J., Li, Z., Dubovik, O., Holben, B., Goloub, P., Chen, H., Estelles, V., Cuevas-Agulló, E., Blarel, L., Wang, H., Zhao, H., Zhang, X., Wang, Y., Sun, J., Tao, R., Zhang, X., and Shi, G.: Column aerosol optical properties and aerosol radiative forcing during a serious haze-fog month over North China Plain in 2013 based on ground-based sunphotometer measurements, Atmos. Chem. Phys., 14, 2125–2138, https://doi.org/10.5194/acp-14-2125-2014, 2014.

Ding, A. J., Huang, X., Nie, W., Sun, J. N., Kerminen, V. M., Petäjä, T., Su, H., Cheng, Y. F., Yang, X. Q., Wang, M. H., Chi, X. G., Wang, J. P., Virkkula, A., Guo, W. D., Yuan, J., Wang, S. Y., Zhang, R. J., Wu, Y. F., Song, Y., Zhu, T., Zilitinkevich, S., Kul-

mala, M., and Fu, C. B.: Enhanced haze pollution by black carbon in megacities in China, Geophys. Res. Lett., 43, 2873–2879, https://doi.org/10.1002/2016GL067745, 2016.

Dong, Z., Li, Z., Yu, X., Cribb, M., Li, X., and Dai, J.: Opposite long-term trends in aerosols between low and high altitudes: a testimony to the aerosol–PBL feedback, Atmos. Chem. Phys., 17, 7997–8009, https://doi.org/10.5194/acp-17-7997-2017, 2017.

Fan, J. and Zhang, R.: Atmospheric oxidation mechanism of isoprene, Environ. Chem., 1, 140–149, 2004.

Fan, J., Zhang, R., Tao, W.-K., and Mohr, K. I.: Effects of aerosol optical properties on deep convective clouds and radiative forcing, J. Geophys. Res., 113, D08209, https://doi.org/10.1029/2007jd009257, 2008.

Guo, S., Hu, M., Zamora, M. L., Peng, J., Shang, D., Zheng, J., Du, Z., Wu, Z., Shao, M., Zeng, L., Molina, M. J., and Zhang, R.: Elucidating severe urban haze formation in China, P. Natl. Acad. Sci. USA, 111, 17373–17378, https://doi.org/10.1073/pnas.1419604111, 2014.

Guo, S., Hu, M., Lin, Y., Gomez-Hernandez, M., Zamora, M. L., Peng, J. F., Collins, D. R., and Zhang, R. Y.: OH-Initiated Oxidation of m-Xylene on Black Carbon Aging, Environ. Sci. Technol., 50, 8605–8612, https://doi.org/10.1021/acs.est.6b01272, 2016.

Guo, S., Hu, M., Peng, J. F., Wu, Z. J., Zamora, M. L., Shang, D. J., Du, Z. F., Zheng, J., Fang, X., Tang, R. Z., Wu, Y. S., Zeng, L. M., Shuai, S. J., Zhang, W. B., Wang, Y., Ji, Y. M., Li, Y. X., Zhang, A. L., Wang, W. G., Zhang, F., Zhao, J. Y., Gong, X. L., Wang, C. Y., Molina, M. J., and Zhang, R. Y.: Remarkable nucleation and growth of ultrafine particles from vehicular exhaust, P. Natl. Acad. Sci. USA, 117, 3427–3432, https://doi.org/10.1073/pnas.1916366117, 2020.

Gustafsson, Ö. and Ramanathan, V.: Convergence on climate warming by black carbon aerosols, P. Natl. Acad. Sci. USA, 113, 4243–4245, https://doi.org/10.1073/pnas.1603570113, 2016.

He, C., Liou, K.-N., Takano, Y., Zhang, R., Levy Zamora, M., Yang, P., Li, Q., and Leung, L. R.: Variation of the radiative properties during black carbon aging: theoretical and experimental intercomparison, Atmos. Chem. Phys., 15, 11967–11980, https://doi.org/10.5194/acp-15-11967-2015, 2015.

Huang, X., Wang, Z., and Ding, A.: Impact of Aerosol-PBL Interaction on Haze Pollution: Multiyear Observational Evidences in North China, Geophys. Res. Lett., 45, 8596–8603, https://doi.org/10.1029/2018GL079239, 2018.

Intergovernmental Panel on Climate Change (IPCC): Climate Change 2013: The Physical Science Basis. Contribution of Working Group I to the Fifth Assessment Report of the Intergovernmental Panel on Climate Change, Cambridge University Press, ISBN 978-92-9169-138-8, 2013.

Ji, Y., Zhao, J., Terazono, H., Misawa, K., Levitt, N. P., Li, Y., Lin, Y., Peng, J., Wang, Y., Duan, L., Pan, B., Zhang, F., Feng, X., An, T., Marrero-Ortiz, W., Secrest, J., Zhang, A. L., Shibuya, K., Molina, M. J., and Zhang, R.: Reassessing the atmospheric oxidation mechanism of toluene, P. Natl. Acad. Sci. USA, 114, 8169–8174, https://doi.org/10.1073/pnas.1705463114, 2017.

Ji, Y., Shi, Q., Li, Y., An, T., Zheng, J., Peng, J., Gao, Y., Chen, J., Li, G., Wang, Y., Zhang, F., Zhang, A. L., Zhao, J., Molina, M. J., and Zhang, R.: Carbenium ion-mediated oligomerization of methylglyoxal for secondary organic aerosol formation, P. Natl. Acad. Sci. USA, 117, 13294–13299, https://doi.org/10.1073/pnas.1912235117, 2020.

Johnson, N. M., Hoffmann, A. R., Behlen, J. C., Lau, C., Pendleton, D., Harvey, N., Shore, R., Li, Y. X., Chen, J. S., Tian, Y. A., and Zhang, R. Y.: Air pollution and children's health-a review of adverse effects associated with prenatal exposure from fine to ultrafine particulate matter, Environ. Health Prev., 26, 72, https://doi.org/10.1186/s12199-021-00995-5, 2021.

Khalizov, A. F., Lin, Y., Qiu, C., Guo, S., Collins, D., and Zhang, R.: Role of OH-initiated oxidation of isoprene in aging of combustion soot, Environ. Sci. Technol., 47, 2254–2263, https://doi.org/10.1021/es3045339, 2013.

Lee, S.-H., Gordon, H., Yu, H., Lehtipalo, K., Haley, R., Li, Y., and Zhang, R.: New Particle Formation in the Atmosphere: From Molecular Clusters to Global Climate, J. Geophys. Res.-Atmos., 124, 7098–7146, https://doi.org/10.1029/2018JD029356, 2019.

Levy, R. C., Leptoukh, G. G., Kahn, R., Zubko, V., Gopalan, A., and Remer, L. A.: A Critical Look at Deriving Monthly Aerosol Optical Depth From Satellite Data, IEEE T. Geosci. Remote, 47, 2942–2956, https://doi.org/10.1109/Tgrs.2009.2013842, 2009.

Li, G., Wang, Y., and Zhang, R.: Implementation of a two-moment bulk microphysics scheme to the WRF model to investigate aerosol-cloud interaction, J. Geophys. Res., 113, D15211, https://doi.org/10.1029/2007jd009361, 2008.

Li, P., Yan, R., Yu, S., Wang, S., Liu, W., and Bao, H.: Reinstate regional transport of $PM_{2.5}$ as a major cause of severe haze in Beijing, P. Natl. Acad. Sci. USA, 112, E2739–E2740, https://doi.org/10.1073/pnas.1502596112, 2015.

Li, Y., Ji, Y., Zhao, J., Wang, Y., Shi, Q., Peng, J., Wang, Y., Wang, C., Zhang, F., Wang, Y., Seinfeld, J. H., and Zhang, R.: Unexpected Oligomerization of Small α-Dicarbonyls for Secondary Organic Aerosol and Brown Carbon Formation, Environ. Sci. Technol., 55, 4430–4439, https://doi.org/10.1021/acs.est.0c08066, 2021a.

Li, Y., Zhao, J., Wang, Y., Seinfeld, J. H., and Zhang, R.: Multigeneration Production of Secondary Organic Aerosol from Toluene Photooxidation, Environ. Sci. Technol., 55, 8592–8603, https://doi.org/10.1021/acs.est.1c02026, 2021b.

Li, Z., Xia, X., Cribb, M., Mi, W., Holben, B., Wang, P., Chen, H., Tsay, S.-C., Eck, T. F., Zhao, F., Dutton, E. G., and Dickerson, R. E.: Aerosol optical properties and their radiative effects in northern China, J. Geophys. Res.-Atmos., 112, D22S01, https://doi.org/10.1029/2006JD007382, 2007.

Li, Z., Guo, J., Ding, A., Liao, H., Liu, J., Sun, Y., Wang, T., Xue, H., Zhang, H., and Zhu, B.: Aerosol and Boundary-Layer Interactions and Impact on Air Quality, Natl. Sci. Rev., 4, 810–833, https://doi.org/10.1093/nsr/nwx117, 2017.

Li, Z. Q., Wang, Y., Guo, J. P., Zhao, C. F., Cribb, M., Dong, X. Q., Fan, J. W., Gong, D. Y., Huang, J. P., Jiang, M. J., Jiang, Y. Q., Lee, S. S., Li, H., Li, J. M., Liu, J. J., Qian, Y., Rosenfeld, D., Shan, S. Y., Sun, Y. L., Wang, H. J., Xin, J. Y., Yan, X., Yang, X., Yang, X. Q., Zhang, F., and Zheng, Y. T.: East Asian Study of Tropospheric Aerosols and their Impact on Regional Clouds, Precipitation, and Climate (EAST-AIR(CPC)), J. Geophys. Res.-Atmos., 124, 13026–13054, https://doi.org/10.1029/2019jd030758, 2019.

Lin, Y., Wang, Y., Pan, B., Hu, J., Liu, Y., and Zhang, R.: Distinct Impacts of Aerosols on an Evolving Continental Cloud Complex

during the RACORO Field Campaign, J. Atmos. Sci., 73, 3681–3700, https://doi.org/10.1175/JAS-D-15-0361.1, 2016.

Liu, J., Zhang, F., Xu, W., Sun, Y., Chen, L., Li, S., Ren, J., Hu, B., Wu, H., and Zhang, R.: Hygroscopicity of organic aerosols linked to formation mechanisms, Geophy. Res. Lett. 48, e2020GL091683, https://doi.org/10.1029/2020GL091683, 2021.

Liu, X. G., Li, J., Qu, Y., Han, T., Hou, L., Gu, J., Chen, C., Yang, Y., Liu, X., Yang, T., Zhang, Y., Tian, H., and Hu, M.: Formation and evolution mechanism of regional haze: a case study in the megacity Beijing, China, Atmos. Chem. Phys., 13, 4501–4514, https://doi.org/10.5194/acp-13-4501-2013, 2013.

Mallet, M., Roger, J. C., Despiau, S., Putaud, J. P., and Dubovik, O.: A study of the mixing state of black carbon in urban zone, J. Geophys. Res.-Atmos., 109, D04202, https://doi.org/10.1029/2003JD003940, 2004.

Meier, J., Wehner, B., Massling, A., Birmili, W., Nowak, A., Gnauk, T., Brüggemann, E., Herrmann, H., Min, H., and Wiedensohler, A.: Hygroscopic growth of urban aerosol particles in Beijing (China) during wintertime: a comparison of three experimental methods, Atmos. Chem. Phys., 9, 6865–6880, https://doi.org/10.5194/acp-9-6865-2009, 2009.

Menon, S., Hansen, J., Nazarenko, L., and Luo, Y.: Climate Effects of Black Carbon Aerosols in China and India, Science, 297, 2250–2253, https://doi.org/10.1126/science.1075159, 2002.

Molina, L. T.: Introductory lecture: air quality in megacities, Faraday Discuss., 226, 9–52, https://doi.org/10.1039/d0fd00123f, 2021.

Nozaki, K. Y.: Mixing Depth Model Using Hourly Surface Observations Report 7053, USAF Environmental Technical Applications Center, 1973.

Pasquill, F.: The Estimation of the Dispersion of Windborne Material, Meteorol. Mag., 90, 33–49, 1961.

Peng, J., Hu, M., Guo, S., Du, Z., Zheng, J., Shang, D., Levy Zamora, M., Zeng, L., Shao, M., Wu, Y.-S., Zheng, J., Wang, Y., Glen, C. R., Collins, D. R., Molina, M. J., and Zhang, R.: Markedly enhanced absorption and direct radiative forcing of black carbon under polluted urban environments, P. Natl. Acad. Sci. USA, 113, 4266–4271, https://doi.org/10.1073/pnas.1602310113, 2016.

Peng, J., Hu, M., Guo, S., Du, Z., Shang, D., Zheng, J., Zheng, J., Zeng, L., Shao, M., Wu, Y., Collins, D., and Zhang, R.: Ageing and hygroscopicity variation of black carbon particles in Beijing measured by a quasi-atmospheric aerosol evolution study (QUALITY) chamber, Atmos. Chem. Phys., 17, 10333–10348, https://doi.org/10.5194/acp-17-10333-2017, 2017.

Peng, J. F., Hu, M., Shang, D. J., Wu, Z. J., Du, Z. F., Tan, T. Y., Wang, Y. N., Zhang, F., and Zhang, R. Y.: Explosive Secondary Aerosol Formation during Severe Haze in the North China Plain, Environ. Sci. Technol., 55, 2189–2207, https://doi.org/10.1021/acs.est.0c07204, 2021.

Petäjä, T., Järvi, L., Kerminen, V. M., Ding, A. J., Sun, J. N., Nie, W., Kujansuu, J., Virkkula, A., Yang, X., Fu, C. B., Zilitinkevich, S., and Kulmala, M.: Enhanced air pollution via aerosol-boundary layer feedback in China, Sci. Rep., 6, 18998, https://doi.org/10.1038/srep18998, 2016.

Platnick, S., King, M., and Hubanks, P.: MODIS Atmosphere L3 Daily Product. NASA MODIS Adaptive Processing System, Goddard Space Flight Center [data set], https://doi.org/10.5067/MODIS/MYD08_D3.061, 2017.

Pope, C. A. and Dockery, D. W.: Health effects of fine particulate air pollution: Lines that connect, J. Air Waste Manage., 56, 709–742, https://doi.org/10.1080/10473289.2006.10464485, 2006.

Qian, Y, Gong, D., Fan, J., Leung, R. L., Bennartz, R., Chen, D., and Wang, W.: Heavy pollution suppresses light rain in China: Observations and modeling, J. Geophys. Res.-Atmos., 114, D00K02, https://doi.org/10.1029/2008JD011575, 2009.

Ramanathan, V., Li, F., Ramana, M. V., Praveen, P. S., Kim, D., Corrigan, C. E., Nguyen, H., Stone, E. A., Schauer, J. J., Carmichael, G. R., Adhikary, B., and Yoon, S. C.: Atmospheric brown clouds: Hemispherical and regional variations in long-range transport, absorption, and radiative forcing, J. Geophys. Res.-Atmos., 112, D22S21, https://doi.org/10.1029/2006JD008124, 2007.

Rychlik, K. A., Secrest, J. R., Lau, C., Pulczinski, J., Zamora, M. L., Leal, J., Langley, R., Myatt, L. G., Raju, M., Chang, R. C. A., Li, Y. X., Golding, M. C., Rodrigues-Hoffmann, A., Molina, M. J., Zhang, R. Y., and Johnson, N. M.: In utero ultrafine particulate matter exposure causes offspring pulmonary immunosuppression, P. Natl. Acad. Sci. USA, 116, 3443–3448, https://doi.org/10.1073/pnas.1816103116, 2019.

Su, T., Li, Z., Li, C., Li, J., Han, W., Shen, C., Tan, W., Wei, J., and Guo, J.: The significant impact of aerosol vertical structure on lower atmosphere stability and its critical role in aerosol–planetary boundary layer (PBL) interactions, Atmos. Chem. Phys., 20, 3713–3724, https://doi.org/10.5194/acp-20-3713-2020, 2020.

Suh, I., Lei, W., and Zhang, R.: Experimental and theoretical studies of isoprene reaction with NO_3, J. Phys. Chem., 105, 6471–6478, 2001.

Sun, Y. L., Jiang, Q., Wang, Z. F., Fu, P. Q., Li, J., Yang, T., and Yin, Y.: Investigation of the Sources and Evolution Processes of Severe Haze Pollution in Beijing in January 2013, J. Geophys Res.-Atmos., 119, 4380–4398, https://doi.org/10.1002/2014jd021641, 2014.

Tang, G., Zhang, J., Zhu, X., Song, T., Münkel, C., Hu, B., Schäfer, K., Liu, Z., Zhang, J., Wang, L., Xin, J., Suppan, P., and Wang, Y.: Mixing layer height and its implications for air pollution over Beijing, China, Atmos. Chem. Phys., 16, 2459–2475, https://doi.org/10.5194/acp-16-2459-2016, 2016.

Tang, W., Qin, J., Yang, K., Liu, S., Lu, N., and Niu, X.: Retrieving high-resolution surface solar radiation with cloud parameters derived by combining MODIS and MTSAT data, Atmos. Chem. Phys., 16, 2543–2557, https://doi.org/10.5194/acp-16-2543-2016, 2016.

Tie, X., Huang, R.-J., Cao, J., Zhang, Q., Cheng, Y., Su, H., Chang, D., Pöschl, U., Hoffmann, T., Dusek, U., Li, G., Worsnop, D. R., and O'Dowd, C. D.: Severe Pollution in China Amplified by Atmospheric Moisture, Sci. Rep., 7, 15760, https://doi.org/10.1038/s41598-017-15909-1, 2017.

Wallace, J. M. and Hobbs, P. V.: Atmospheric Science, 2nd edn., Elsevier, ISBN 9780127329512, 2005.

Wang, G., Zhang, R., Gomez, M. E., Yang, L., Levy Zamora, M., Hu, M., Lin, Y., Peng, J., Guo, S., Meng, J., Li, J., Cheng, C., Hu, T., Ren, Y., Wang, Y., Gao, J., Cao, J., An, Z., Zhou, W., Li, G., Wang, J., Tian, P., Marrero-Ortiz, W., Secrest, J., Du, Z., Zheng, J., Shang, D., Zeng, L., Shao, M., Wang, W., Huang, Y., Wang, Y., Zhu, Y., Li, Y., Hu, J., Pan, B., Cai, L., Cheng, Y., Ji, Y., Zhang, F., Rosenfeld, D., Liss, P. S., Duce, R. A., Kolb, C. E., and Molina, M. J.: Persistent sulfate formation from London Fog

to Chinese haze, P. Natl. Acad. Sci. USA, 113, 13630–13635, https://doi.org/10.1073/pnas.1616540113, 2016.

Wang, H., Shi, G. Y., Zhang, X. Y., Gong, S. L., Tan, S. C., Chen, B., Che, H. Z., and Li, T.: Mesoscale modelling study of the interactions between aerosols and PBL meteorology during a haze episode in China Jing–Jin–Ji and its near surrounding region – Part 2: Aerosols' radiative feedback effects, Atmos. Chem. Phys., 15, 3277–3287, https://doi.org/10.5194/acp-15-3277-2015, 2015.

Wang, J., Allen, D. J., Pickering, K. E., Li, Z., and He, H.: Impact of aerosol direct effect on East Asian air quality during the EAST-AIRE campaign, J. Geophys. Res.-Atmos., 121, 6534–6554, https://doi.org/10.1002/2016JD025108, 2016.

Wang, Y., Che, H., Ma, J., Wang, Q., Shi, G., Chen, H., Goloub, P., and Hao, X.: Aerosol radiative forcing under clear, hazy, foggy, and dusty weather conditions over Beijing, China, Geophys. Res. Lett., 36, L06804, https://doi.org/10.1029/2009GL037181, 2009.

Wang, Y., Wan, Q., Meng, W., Liao, F., Tan, H., and Zhang, R.: Long-term impacts of aerosols on precipitation and lightning over the Pearl River Delta megacity area in China, Atmos. Chem. Phys., 11, 12421–12436, https://doi.org/10.5194/acp-11-12421-2011, 2011.

Wang, Y., Khalizov, A., Levy, M., and Zhang, R. Y.: New Directions: Light absorbing aerosols and their atmospheric impacts, Atmos. Environ., 81, 713–715, https://doi.org/10.1016/j.atmosenv.2013.09.034, 2013.

Wang, Y., Lee, K.-H., Lin, Y., Levy, M., and Zhang, R.: Distinct effects of anthropogenic aerosols on tropical cyclones, Nat. Clim. Change, 4, 368–373, https://doi.org/10.1038/nclimate2144, 2014a.

Wang, Y., Wang, M., Zhang, R., Ghan, S. J., Lin, Y., Hu, J., Pan, B., Levy, M., Jiang, J. H., and Molina, M. J.: Assessing the effects of anthropogenic aerosols on Pacific storm track using a multiscale global climate model, P. Natl. Acad. Sci. USA, 111, 6894–6899, https://doi.org/10.1073/pnas.1403364111, 2014b.

Wang, Y., Zhang, R., and Saravanan, R.: Asian pollution climatically modulates mid-latitude cyclones following hierarchical modelling and observational analysis, Nat. Commun., 5, 3098, https://doi.org/10.1038/ncomms4098, 2014c.

Wang, Y. S., Yao, L., Wang, L. L., Liu, Z. R., Ji, D. S., Tang, G. Q., Zhang, J. K., Sun, Y., Hu, B., and Xin, J. Y.: Mechanism for the Formation of the January 2013 Heavy Haze Pollution Episode over Central and Eastern China, Sci. China Earth Sci., 57, 14–25, https://doi.org/10.1007/s11430-013-4773-4, 2014.

Wang, Z., Huang, X., and Ding, A.: Dome effect of black carbon and its key influencing factors: a one-dimensional modelling study, Atmos. Chem. Phys., 18, 2821–2834, https://doi.org/10.5194/acp-18-2821-2018, 2018.

Wang, Z. L., Zhang, H., and Zhang, X. Y.: Simultaneous reductions in emissions of black carbon and co-emitted species will weaken the aerosol net cooling effect, Atmos. Chem. Phys., 15, 3671–3685, https://doi.org/10.5194/acp-15-3671-2015, 2015.

Wilcox, E. M., Thomas, R. M., Praveen, P. S., Pistone, K., Bender, F. A.-M., and Ramanathan, V.: Black carbon solar absorption suppresses turbulence in the atmospheric boundary layer, P. Natl. Acad. Sci. USA, 113, 11794–11799, https://doi.org/10.1073/pnas.1525746113, 2016.

Wood, E. C., Canagaratna, M. R., Herndon, S. C., Onasch, T. B., Kolb, C. E., Worsnop, D. R., Kroll, J. H., Knighton, W. B., Seila, R., Zavala, M., Molina, L. T., DeCarlo, P. F., Jimenez, J. L., Weinheimer, A. J., Knapp, D. J., Jobson, B. T., Stutz, J., Kuster, W. C., and Williams, E. J.: Investigation of the correlation between odd oxygen and secondary organic aerosol in Mexico City and Houston, Atmos. Chem. Phys., 10, 8947–8968, https://doi.org/10.5194/acp-10-8947-2010, 2010.

Wu, G., Li, Z., Fu, C., Zhang, X., Zhang, R., Zhang, R., Zhou, T., Li, J., Li, J., Zhou, D., Wu, L., Zhou, L., He, B., and Huang, R.: Advances in studying interactions between aerosols and monsoon in China, Sci. China Earth Sci., 59, 1–16, https://doi.org/10.1007/s11430-015-5198-z, 2016.

Wu, G. Y., Brown, J., Zamora, M. L., Miller, A., Satterfield, M. C., Meininger, C. J., Steinhauser, C. B., Johnson, G. A., Burghardt, R. C., Bazer, F. W., Li, Y. X., Johnson, N. M., Molina, M. J., and Zhang, R. Y.: Adverse organogenesis and predisposed long-term metabolic syndrome from prenatal exposure to fine particulate matter, P. Natl. Acad. Sci. USA, 116, 11590–11595, https://doi.org/10.1073/pnas.1902925116, 2019.

Wu, J. R., Bei, N. F., Hu, B., Liu, S. X., Wang, Y., Shen, Z. X., Li, X., Liu, L., Wang, R. N., Liu, Z. R., Cao, J. J., Tie, X. X., Molina, L. T., and Li, G. H.: Aerosol-photolysis interaction reduces particulate matter during wintertime haze events, P. Natl. Acad. Sci. USA, 117, 9755–9761, https://doi.org/10.1073/pnas.1916775117, 2020.

Xia, X., Chen, H., Goloub, P., Zhang, W., Chatenet, B., and Wang, P.: A compilation of aerosol optical properties and calculation of direct radiative forcing over an urban region in northern China, J. Geophys. Res.-Atmos., 112, D12203, https://doi.org/10.1029/2006JD008119, 2007.

Xu, W. and Zhang, R.: Theoretical investigation of interaction of dicarboxylic acids with common aerosol nucleation precursors, J. Phys. Chem., 116, 4539–4550, https://doi.org/10.1021/jp301964u, 2012.

Yuan, T., Li, Z., Zhang, R., and Fan, J.: Increase of cloud droplet size with aerosol optical depth: An observation and modeling study, J. Geophys. Res., 113, D04201, https://doi.org/10.1029/2007JD008632, 2008.

Zhang, F., Wang, Y., Peng, J. F., Chen, L., Sun, Y. L., Duan, L., Ge, X. L., Li, Y. X., Zhao, J. Y., Liu, C., Zhang, X. C., Zhang, G., Pan, Y. P., Wang, Y. S., Zhang, A. L., Ji, Y. M., Wang, G. H., Hu, M., Molina, M. J., and Zhang, R. Y.: An unexpected catalyst dominates formation and radiative forcing of regional haze, P. Natl. Acad. Sci. USA, 117, 3960–3966, https://doi.org/10.1073/pnas.1919343117, 2020.

Zhang, R., Li, G. H., Fan, J. W., Wu, D. L., and Molina, M. J.: Intensification of Pacific storm track linked to Asian pollution, P. Natl. Acad. Sci. USA, 104, 5295–5299, https://doi.org/10.1073/pnas.0700618104, 2007.

Zhang, R., Khalizov, A. F., Pagels, J., Zhang, D., Xue, H., and McMurry, P. H.: Variability in morphology, hygroscopicity, and optical properties of soot aerosols during atmospheric processing, P. Natl. Acad. Sci. USA, 105, 10291–10296, https://doi.org/10.1073/pnas.0804860105, 2008.

Zhang, R., Wang, L., Khalizov, A. F., Zhao, J., Zheng, J., McGraw, R. L., and Molina, L. T.: Formation of nanoparticles of blue haze enhanced by anthropogenic pollution, P. Natl. Acad. Sci. USA, 106, 17650–17654, https://doi.org/10.1073/pnas.0910125106, 2009.

Zhang, R., Guo, S., Levy Zamora, M., and Hu, M.: Reply to Li et al.: Insufficient evidence for the contribution of regional transport to severe haze formation in Beijing, P. Natl. Acad. Sci. USA, 112, E2741, https://doi.org/10.1073/pnas.1503855112, 2015a.

Zhang, R., Wang, G., Guo, S., Zamora, M. L., Ying, Q., Lin, Y., Wang, W., Hu, M., and Wang, Y.: Formation of Urban Fine Particulate Matter, Chem. Rev., 115, 3803–3855, https://doi.org/10.1021/acs.chemrev.5b00067, 2015b.

Zhang, R., Johnson, N. M., and Li, Y.: Establishing the exposure-outcome relation between airborne particulate matter and children's health, Thorax, 76, 322–323, https://doi.org/10.1136/thoraxjnl-2021-217017, 2021.

Zhang, X., Zhang, Q., Hong, C., Zheng, Y., Geng, G., Tong, D., Zhang, Y., and Zhang, X.: Enhancement of $PM_{2.5}$ concentrations by aerosol-meteorology interactions over China, J. Geophys. Res.-Atmos., 1179–1194, https://doi.org/10.1002/2017JD027524, 2018.

Zhao, J., Zhang, R., Fortner, E. C., and North, S. W.: Quantification of hydroxycarbonyls from OH-isoprene reactions, J. Am. Chem. Soc., 126, 2686–2687, 2004.

Zhao, J., Zhang, R., Misawa, K., and Shibuya, K.: Experimental product study of the OH-initiated oxidation of m-xylene, J. Photoch. Photobio. A, 176, 199–207, 2005.